Increased arterial stiffness and extracellular matrix reorganization in intrauterine growth–restricted fetal sheep

Reuben Blair Dodson[1], Paul J. Rozance[2], Bradley S. Fleenor[3], Carson C. Petrash[1], Lauren G. Shoemaker[4], Kendall S. Hunter[5] and Virginia L. Ferguson[1,6]

BACKGROUND: Fetal intrauterine growth restriction (IUGR) results in increased placental resistance to blood flow, fetal hypertension, and increased pulsatility stresses shown to lead to vascular remodeling. We tested our hypothesis that IUGR causes decreased compliance in the carotid and umbilical arteries due to altered extracellular matrix (ECM) composition and structure.
METHODS: A sheep model of placental insufficiency–induced IUGR (PI-IUGR) was created by exposure of the pregnant ewe to elevated ambient temperatures. Umbilical and carotid arteries from near-term fetuses were tested with pressure–diameter measurements to compare passive compliance in control and PI-IUGR tissues. ECM composition was measured via biochemical assay, and the organization was determined by using histology and second-harmonic generation imaging.
RESULTS: We found that PI-IUGR increased arterial stiffness with increased collagen engagement, or transition stretch. PI-IUGR carotid arteries exhibited increased collagen and elastin quantity, and PI-IUGR umbilical arteries exhibited increased sulfated glycosaminoglycans. Histomorphology showed altered collagen-to-elastin ratios with altered cellular proliferation. Increased stiffness indicates altered collagen-to-elastin ratios with less elastin contribution leading to increased collagen engagement.
CONCLUSION: Because vessel stiffness is a significant predictor in the development of hypertension, disrupted ECM deposition in IUGR provides a potential link between IUGR and adult hypertension.

In adolescents and adults, increased stiffness in large elastic arteries is a significant contributor to the progression of cardiovascular disease (CVD) (1–3). The extracellular matrix (ECM) that defines arterial stiffness rapidly forms during late gestation and in the newborn. Smooth muscle cells regulate the development of ECM to meet the biomechanical demands of the systemic arteries by signaling changes with respect to increases in blood pressure and hemodynamic flows within a vessel (4). Elastin, the ECM component that provides elasticity and low-pressure strength in blood vessels, has been shown to rapidly accumulate during the late gestation and early neonatal period and to degrade slowly as individuals age (5–7). Collagen, a much stiffer ECM component, is deposited to accommodate increased biomechanical loading as blood pressure increases or under increased shear stress, as with aging or disease (4–7). Proteoglycans are a small but important part of the ECM that consist of a core protein to which multiple glycosaminoglycan (GAG) chains are covalently attached and have the ability to incorporate water and viscosity to the tissue. Adaptations in vascular formation to short-term complications from maternal stress, such as intrauterine growth restriction (IUGR), *in utero* could directly impact adult cardiovascular health through altered vascular growth and remodeling of any of these components of the ECM.

IUGR is a common complication of human pregnancies and results in both short- and long-term complications. In the short-term, IUGR is associated with altered hemodynamics as a result of increased placental resistance to blood flow and increased fetal arterial blood pressure (8,9), whereas long-term complications include a predisposition toward the development of CVD (10,11). However, the mechanisms linking IUGR with adult-onset CVD remain incompletely understood and more research is needed to understand the pathogenesis of abnormal fetal vascular development IUGR.

In humans, Burkhardt *et al.*(5) showed that IUGR newborns have reduced umbilical artery compliance. Furthermore, Burkhardt argued that as an extension of the fetal cardiovascular system and the only vessel readily available for *in vitro* study in humans, the umbilical arteries provided a snapshot of fetal vascular development (5). But whether this is true in IUGR remains untested.

We hypothesized that IUGR near-term fetuses have increased carotid and umbilical arterial stiffness due to altered ECM composition and organization caused by increased hemodynamic stresses as compared with that of normal fetuses. For this study, we used a sheep model of placental insufficiency that results in IUGR fetuses characterized by hemodynamic changes and many other complications seen in severe human

The last two authors are senior authors.
[1]Department of Mechanical Engineering, University of Colorado at Boulder, Boulder, Colorado; [2]Department of Pediatrics, University of Colorado School of Medicine, Aurora, Colorado; [3]Department of Integrative Physiology, University of Colorado at Boulder, Boulder, Colorado; [4]Biofrontiers Institute, University of Colorado, Boulder, Colorado; [5]Department of Bioengineering, University of Colorado at Denver, Anschutz Medical Campus, Aurora, Colorado; [6]Department of Obstetrics and Gynecology, University of Colorado at Denver, Anschutz Medical Campus, Aurora, Colorado. Correspondence: Virginia L. Ferguson (virginia.ferguson@colorado.edu)

Received 21 May 2012; accepted 6 September 2012; advance online publication 12 December 2012. doi:10.1038/pr.2012.156

Table 1. Necropsy values for PI-IUGR and control animals

	CON ($n = 12$)	IUGR ($n = 9$)	%	
	Mean ± SEM	Mean ± SEM	Change	*P* value
Necropsy data				
Fetal weight (g)	3,318.3 ± 176.5	2,129.7 ± 172.9	↓36%	0.0002*
Placental weight (g)	465.3 ± 46.5	226.1 ± 16.7	↓51%	0.002*
Age at necropsy (d)	134 ± 1	133 ± 1		0.28
Crown-to-rump length (mm)	477 ± 12	409 ± 9	↓14%	0.0004*
Sex				
Female, *n* (%)	6 (50%)	4 (45%)		
Male, *n* (%)	6 (50%)	5 (55%)		
Normalized heart weight	5.9 ± 0.4	6.7 ± 0.3		0.16
Left ventricle and septum (g/kg)	2.6 ± 0.2	3.1 ± 0.1	↑18%	0.041*
Right ventricle (g/kg)	1.3 ± 0.1	1.5 ± 0.1		0.23
Atria and great vessels (g/kg)	2.0 ± 0.2	2.1 ± 0.2		0.67
Arterial morphology				
Carotid inner diameter (mm)	1.83 ± 0.11	2.25 ± 0.18	↑23%	0.045*
Carotid thickness (mm)	0.54 ± 0.04	0.39 ± 0.03	↓28%	0.011*
Umbilical inner diameter (mm)	1.02 ± 0.09	1.03 ± 0.13		0.97
Umbilical thickness (mm)	0.96 ± 0.06	1.01 ± 0.05		0.58

CON, control; IUGR, intrauterine growth restriction.

*Significant at $P < 0.05$ by Student's *t*-test, except that Mann–Whitney nonparametric test was run for placental weight.

IUGR (8–9,12).This sheep model of placental insufficiency-IUGR (PI-IUGR) replicates a naturally occurring phenomenon in which gestation in elevated ambient temperatures reduces placental transport size and function, a hallmark of IUGR (12). Similarities of reduced growth, disrupted metabolism, and altered hemodynamics between the sheep PI-IUGR and human IUGR have been noted (8). This model of PI-IUGR is characterized by elevated fetal blood pressure, increased pulsatility in the fetal umbilical and descending aorta arteries, and increased placental resistance to fetal umbilical blood flow (9). In the current study, we measured arterial stiffness in isolated umbilical cord and fetal carotid arteries as well as ECM composition and organization to elucidate the contribution of IUGR to vascular development.

RESULTS

Animal Morphology

The PI-IUGR fetuses had significant growth restriction, with lower fetal weight, placental weight, and crown-to-rump length

Figure 1. Movat's pentachrome histology. Movat's pentachrome–stained cross-sections for representative (**a**) carotid arteries (left side: control panel and right side: placental insufficiency–induced intrauterine growth restriction (PI-IUGR) panel; bar = 100 μm) and (**b**) umbilical arteries (left side: control panel and right side: PI-IUGR panel; bar = 200 μm). Qualitative analysis showed PI-IUGR arteries had media with increased ground substance (GAGs), and the adventitia exhibited increased collagen disrupting the collagen-to-elastin ratio, indicating arterial stiffening. GAGs, glycosaminoglycans.

(Table 1). The normalized left-ventricular weight (grams per kilogram fetal weight) was 18% higher in the PI-IUGR fetuses. The unpressurized and unstretched PI-IUGR carotid arteries showed a 23% increase in inner diameter and a 28% decrease in wall thickness as compared with controls. The unpressurized and unstretched umbilical artery demonstrated no change in inner diameter and wall thickness, despite the reduced fetal size and placental insufficiency (Table 1).

Movat's Pentachrome

Initial Movat's pentachrome stain (Figure 1) qualitatively showed the PI-IUGR media has more ground substance: hydrophilic sulfated GAGs and altered cellular quantity as compared with the control. PI-IUGR arteries exhibited more collagen in the adventitia. Given these qualitative changes and the qualitative nature of this analysis, we next performed quantitative biomechanical, morphological, and biochemical assays.

Arterial Stiffness

In PI-IUGR, both carotid and umbilical arteries were significantly less compliant as compared with controls at equivalent pressures as indicated by the leftward shift in the collagen engagement (Figure 2). At equivalent pressures, the circumferential stretch is less in the PI-IUGR carotid arteries for pressures 70–200 mm Hg and in the umbilical arteries for pressures 40–200 mm Hg ($P < 0.05$). The transition stretch ($\lambda_{stretch}$), which describes the elastin contribution and the initiation of collagen engagement in the compliance, was significantly lower in both the PI-IUGR carotid and umbilical arteries as compared with the control (Figure 2c,d).

ECM Composition

The PI-IUGR carotid artery had more collagen and elastin content. The PI-IUGR umbilical artery had no change in collagen or elastin content but had less sulfated GAG content (Table 2). Quantification of the hematoxylin and eosin–stained images (Figure 3) showed higher cell number in the carotid artery (control (CON) = 0.28 ± 0.04; IUGR = 0.40 ± 0.02 cell nuclei/100 μm^2; $P < 0.05$) and lower cell number in the umbilical artery (CON = 0.28 ± 0.02; IUGR = 0.19 ± 0.02

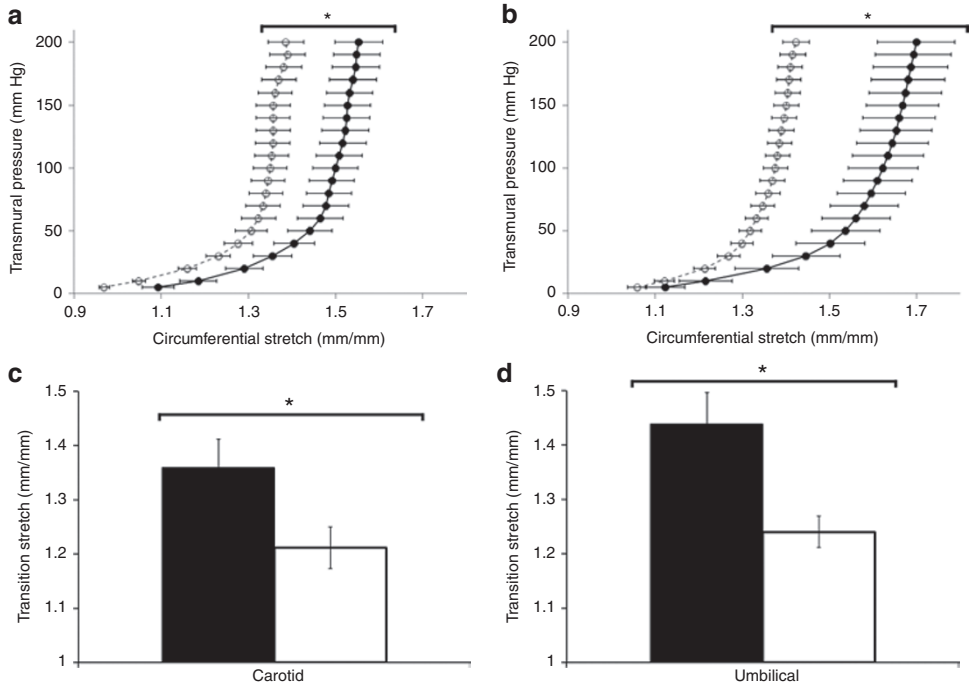

Figure 2. (**a**–**b**) Pressure vs. circumferential stretch for control (black circles) and placental insufficiency–induced intrauterine growth restriction (PI-IUGR) (white circles) samples. *Significant difference between groups ($P < 0.05$). (**a**) Carotid artery is significantly different at pressures between 70 and 200 mm Hg ($P < 0.05$). (**b**) Umbilical artery is significantly different at pressures between 40 and 200 mm Hg ($P < 0.05$). Previous research has shown that the mean systemic blood pressures in this breed of animal are 44.5 and 50.2 mm Hg, for control and PI-IUGR animals, respectively (9). (**c**–**d**) Transition circumferential stretch quantifying elastin and collagen engagement mechanics for control (black squares) and PI-IUGR (white squares). (**c**) Carotid and (**d**) umbilical arteries display lower transition stretch.

Table 2. Biochemical assay data

	Control	IUGR	%	*P*
	Mean ± SEM	Mean ± SEM	Change	value
Carotid artery				
Hydroxyproline (μg/mg)	85.7 ± 5.5	108.6 ± 10.6	↑27%	0.004*
Desmosine (μg/mg)	2.10 ± 0.18	2.95 ± 0.17	↑40%	0.001*
Sulfated GAGs (μg/mg)	25.4 ± 1.1	22.8 ± 1.2		0.13
Umbilical artery				
Hydroxyproline (μg/mg)	85.4 ± 5.1	83.8 ± 6.2		0.72
Desmosine (μg/mg)	0.73 ± 0.07	0.94 ± 0.14		0.19
Sulfated GAGs (μg/mg)	26.9 ± 0.9	22.5 ± 1.7	↓16%	0.040*

GAGs, glycosaminoglycans; IUGR, intrauterine growth restriction.

*Significant at $P < 0.05$ by Student's *t*-test.

cell nuclei/100 μm^2; $P < 0.05$) in PI-IUGR. Quantification of the area fraction of elastin in Verhoeff-van Gieson images (**Figure 4**) showed a lower proportion of elastin to arterial wall area in the carotid (CON = 27.4 ± 2.1%; IUGR = 19.2 ± 2.2%; $P < 0.05$) and umbilical (CON = 10.8 ± 0.9%; IUGR = 7.2 ± 1.2%; $P < 0.05$) arteries in PI-IUGR (**Figure 4**). However, the absolute total area of elastin remained the same between groups.

High-resolution second-harmonic generation (SHG) images of representative PI-IUGR carotid arteries qualitatively exhibited a reorganized adventitia that contained increased elastin and increased collagen (**Figure 5a**). The media of the PI-IUGR carotid (**Figure 5a**) arteries exhibited fewer elastic lamellae, or elastin bands, per area as compared with the control vessels and were also noted to be thinner than the control carotid arteries. The SHG PI-IUGR umbilical arteries (**Figure 5b**), which contained less elastin area than the carotid, showed thinner, less banded internal elastic lamina. The PI-IUGR media had less organized, more fragmented elastin as compared with the control umbilical arteries (**Figure 5b**).

DISCUSSION

The aim of our study was to determine differences in the growth and remodeling of systemic arteries at the end of gestation between control and PI-IUGR fetuses by testing the passive compliance and the structural ECM components. The ECM responds to the biomechanical environment, providing a snapshot of hemodynamic changes occurring during development. The important findings of our study are as follows: (i) less compliant carotid and umbilical arteries in PI-IUGR fetuses and lower transition stretch, demonstrating the reduced elastin and increased collagen contribution to arterial mechanics; (ii) the PI-IUGR carotid had significantly higher collagen and elastin biochemical quantity as compared with the controls whereas umbilical vessels had lower sulfated GAG content; (iii) PI-IUGR carotid arteries showed a change in morphology, exhibiting a larger inner diameter and thinner walls whereas PI-IUGR umbilical arteries showed no change, despite a decrease in fetal size; and (iv) ECM organization changed, as demonstrated by less elastin area and elastin fibers that appeared more fragmented

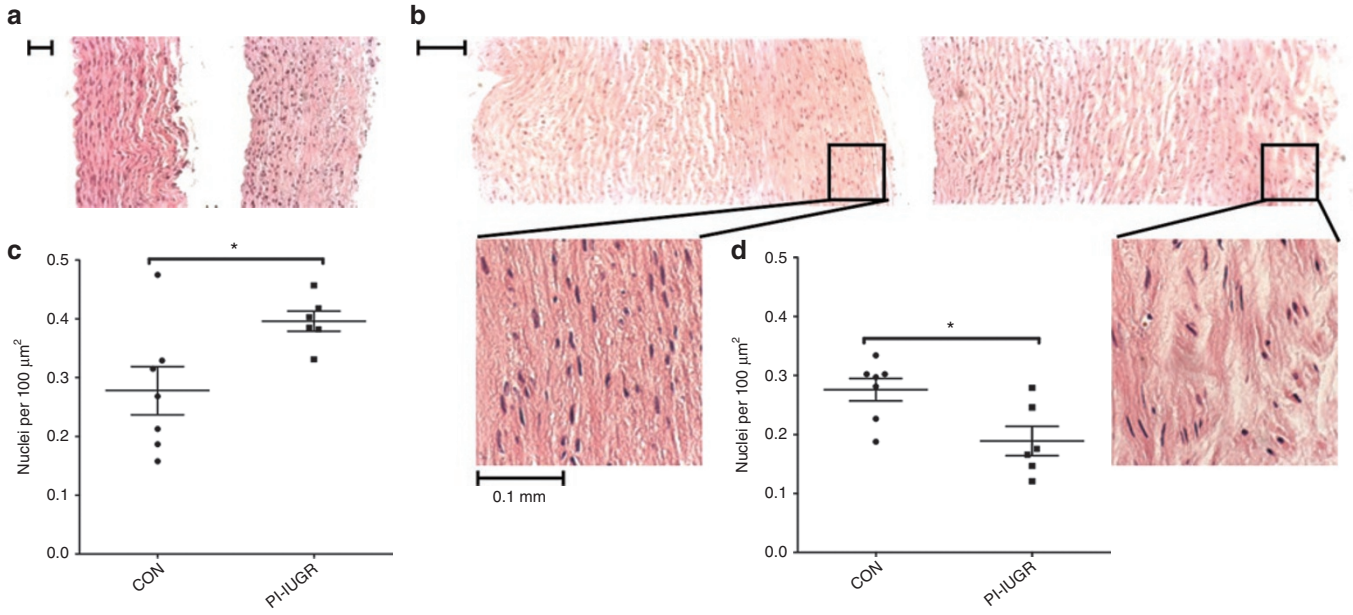

Figure 3. Hematoxylin and eosin (H&E) histology and analysis. H&E-stained cross-sections for representative (**a**) carotid arteries (left side: control panel and right side: placental insufficiency–induced intrauterine growth restriction (PI-IUGR) panel; bar = 100 μm) and (**b**) umbilical arteries (left side: control panel and right side: PI-IUGR panel; bar = 200 μm). Quantification for number of nuclei per 100 μm² for (**c**) the largely elastic carotid arteries show increased cell nuclei per area (*$P < 0.05$), but (**d**) the largely muscular umbilical arteries show decreased cell nuclei per area (*$P < 0.05$).

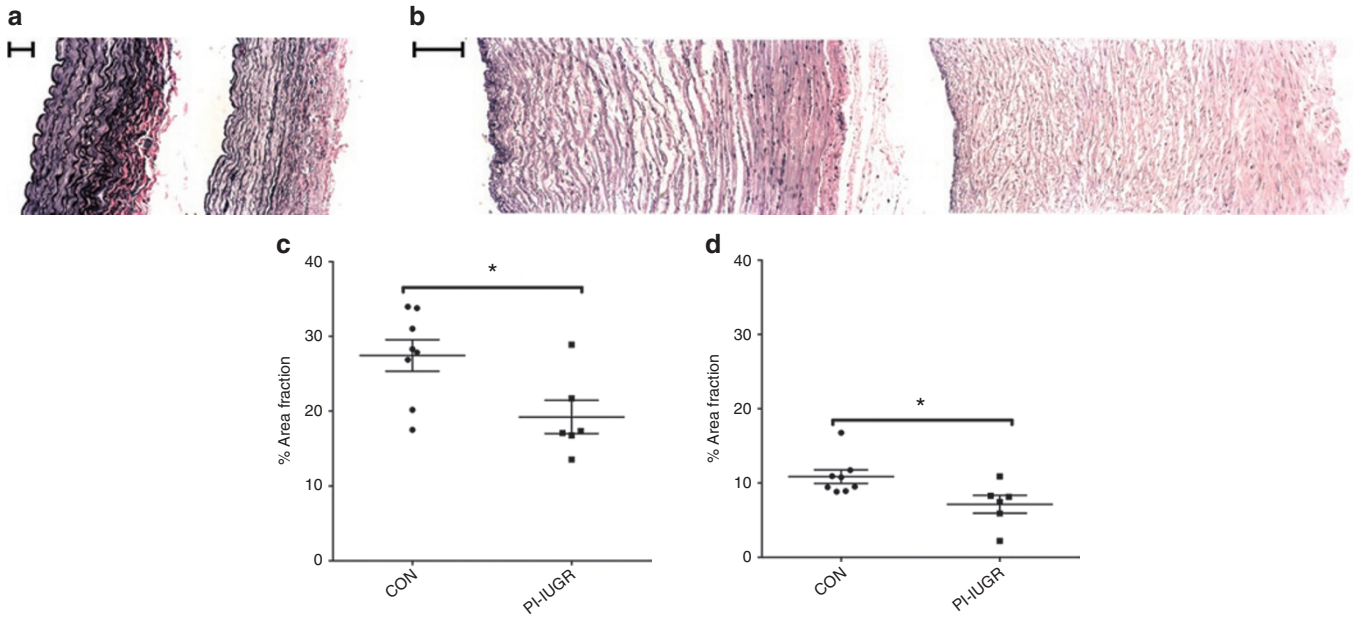

Figure 4. Verhoeff-van Gieson (VVG) histology and analysis. VVG-stained cross-sections for representative (**a**) carotid arteries (left side: control panel and right side: placental insufficiency–induced intrauterine growth restriction (PI-IUGR) panel; bar = 100 μm) and (**b**) umbilical arteries (left side: control panel and right side: PI-IUGR panel; bar = 200 μm). Elastin area fraction measures the collagen-to-elastin ratio. The (**c**) carotid and (**d**) umbilical arteries showed reduced area of elastin to total arterial wall area (*$P < 0.05$), demonstrating reorganization of collagen and elastin.

and disorganized in the PI-IUGR vessels, with more cellularity in the carotid and less cellularity in the umbilical artery.

For the fetus and subsequent neonate, stiffer vessels result in reduced arterial function. Arterial stiffening means less Windkessel effect, or elastic reservoir, available to store potential energy required for steady flow to the organ beds. The heart functions as an intermittent pump, which discharges blood flow only during systole. Therefore, arterial elasticity is critical in promoting forward laminar, less pulsatile hemodynamic flow in these large elastic conduit arteries and reducing left ventricle afterload (3). The PI-IUGR arteries had higher collagen content, altering the collagen-to-elastin ratio as seen in the Verhoeff-van Gieson histomorphology. Higher collagen content in the PI-IUGR carotid artery disrupts the normal

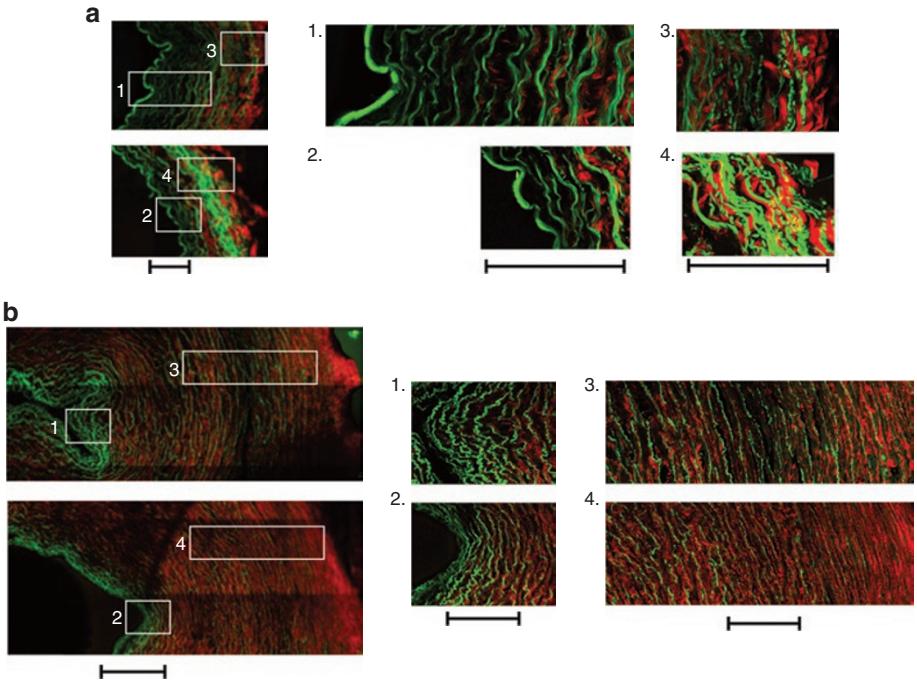

Figure 5. Second-harmonic generation. Arterial sections shown in the axial plane for representative (**a**) carotid arteries (top: control panel and bottom: placental insufficiency–induced intrauterine growth restriction (PI-IUGR) panel; bar = 100 μm) with autofluorescence of collagen (red) and elastin (green). Qualitative images show that, as compared with the control vessels (1) (bar = 100 μm), PI-IUGR (2) arteries exhibited disrupted extracellular matrix (ECM) organization with media of fewer elastic lamellae, or elastin bands, per area. As compared with the control arteries (3) (bar = 100 μm), the external elastic lamina and adventitia of the PI-IUGR (4) arteries exhibited more elastin that was less organized and more fragmented, and increased collagen. Representative (**b**) umbilical arteries (top: control panel and bottom: PI-IUGR panel; bar = 200 μm) show that, as compared with the control vessels (1) (bar = 100 μm), PI-IUGR (2) arteries exhibited disrupted ECM organization with media of fewer elastic lamellae per area. As compared with the control arteries (3) (bar = 100 μm), the external media of the PI-IUGR (4) arteries exhibited more elastin that was less organized and more fragmented, and increased collagen.

collagen-to-elastin ratio, stiffening the arterial compliance and reducing the elastin area fraction. In the umbilical artery, less sulfated GAGs in the PI-IUGR artery create less viscous dissipating energy in addition to reducing compliance. The reduction of GAGs appears to have an important role in the poromechanics (13), with the PI-IUGR umbilical vessels exhibiting stiffness as compared with the control vessels. **Figure 1** shows a qualitative remodeling with a decrease in smooth muscle cells (red) and increase in ground substance (blue) based on observational colorimetric analysis. However, more traditional metrics of histomorphology and biochemical analysis were used to understand changes vs. the less reliable, widely variable Movat's pentachrome staining. The remodeling in PI-IUGR arteries leads to increased stiffness, which has been shown to cause altered hemodynamics and resistance to flow, producing left ventricle hypertrophy (14,15).

Arterial growth and development is critical during the fetal and neonatal periods, with the majority of collagen and elastin deposition occurring at this time (6,7). In the PI-IUGR model, vascular development appears to be influenced by increased placental resistance, blood pressure, and hemodynamics. IUGR increases relative blood flow to the brain to "spare" this vital organ (8), leading to the observed change in the unstressed carotid artery morphology in our study. The unstressed umbilical artery size in the PI-IUGR model remained normal.

The passive compliance is defined principally by the ECM structural constituents collagen and elastin. These passive constituents provide the major structural elements for the arterial biomechanics and are deposited and oriented dependent on pressure and flow (16–19). GAGs function to increase viscous energy dissipation, which reduces stiffness, in response to biomechanical loading (20). Together, these ECM structural components are well documented to contribute to the functional pressure–diameter curves. Arterial health is dependent on having the correct collagen-to-elastin ratio, given that elastin deficiency leads to higher blood pressure and pulsatility (21). Studies of the human umbilical arteries in IUGR using histologic staining have revealed no change in biochemical elastin content but decreased percentage area fraction of elastin, contributing to stiffer arterial walls (5). Recent studies have shown reduced elastin area and increased collagen area in aorta of the hypoxic sheep fetus (22) and increased collagen content with increased stiffness in adult PI-IUGR guinea pig (23). Researchers have hypothesized that in fetuses whose growth is impaired, the synthesis of elastin in the walls of the aorta and large arteries may be deficient, thus leading to permanent changes in the compliance properties of these vessels and predisposing an individual to CVD (24–27). Our results show that the carotid and umbilical arteries have less elastic reservoir, less apparent

elastin contribution, and more apparent collagen content and engagement. Histomorphology and SHG images show reorganization of ECM in PI-IUGR, leading to the reduced compliance. Increased vessel stiffness represents a complex interplay of functional and structural contributions that determine vessel compliance. Therefore, both concentration and organization of the ECM contribute to arterial biomechanical function and are susceptible to disease.

This first report of elastin and collagen remodeling in large elastic arteries in a PI-IUGR sheep model contributes to understanding the long-term impact of IUGR on CVD. Burkhardt *et al.*(5) suggested that the human IUGR umbilical artery could provide insight into the fetal vasculature. Using a well-established sheep model of PI-IUGR allowed a direct comparison of neonatal systemic vessels against the umbilical artery. Our data support this idea of using the umbilical artery as a snapshot of systemic arterial remodeling absent an animal model, as we found decreased compliance in the carotid artery as well as in the umbilical artery. However, we also found differences between the effects of placental insufficiency on the carotid and umbilical arteries (ECM composition, morphology, and cellularity). This pattern of physical changes demonstrates the continuing need to use animal models of IUGR to fully understand vascular development in IUGR. The cardiovascular development in a large animal model of health and disease provides insight into the role of arterial stiffening, which has been shown to be critical in the pathogenesis of CVD (28–31). Specifically, our data provide compelling animal evidence to partially explain the epidemiological and observational studies in humans linking IUGR and developmental origins of CVD (10,11,32,33).

Future studies will determine the extent of abnormal systemic arterial growth and remodeling in the IUGR fetus and the role hemodynamic stress plays as a signaling mechanism. Furthermore, we report results for the near-term fetus. It is still uncertain when abnormal arterial growth and remodeling begins, and the long-term consequences of vessel stiffening in this model of PI-IUGR are also unknown. However, our data provide an initial basis for the development of a constitutive model to relate changes in arterial microstructure to biomechanical function in IUGR fetuses. Such constitutive models have the ability to aid our understanding of the relationship between vessel stiffening and altered blood flow characteristics. Future studies are also necessary to understand the roles of mechanical stress and biochemical signaling, the biochemomechanical pathways leading to arterial growth and remodeling in the IUGR fetus.

In conclusion, PI results in IUGR and reduces both carotid and umbilical arterial compliance. The decreased compliance is associated with previously measured increased fetal blood pressure, placental resistance, and arterial pulsatility. We also found that the arterial remodeling occurs in PI-IUGR mainly via increased collagen and elastin content in the carotid artery and decreased sulfated GAGs in the umbilical artery with altered collagen-to-elastin ratio. Overall, these data provide a potential mechanism between IUGR and adult CVD.

MATERIALS AND METHODS

Animal Model

This study was performed in pregnant Columbia–Rambouillet ewes at the Perinatal Research Center at the University of Colorado School of Medicine and approved by the institutional animal care and use committee. The Perinatal Research Center is accredited by the National Institutes of Health, the United States Department of Agriculture, and the American Association for Accreditation of Laboratory Animal Care. PI-IUGR ($n = 9$) was created by exposure of pregnant ewes to elevated ambient temperatures (40 °C for 12 h; 35° for 12 h) for ~80 d (from 35 to 112 d gestational age; term = 148 d gestational age) as previously described (8,12,34,35). Following this exposure, ewes were housed in a normothermic environment (20 °C) for the remainder of the study. CON) ($n = 12$) ewes were housed in a normothermic environment for the duration of the study.

Mechanical Testing

The ewe and fetus were anesthetized with ketamine (1,000 mg) and diazepam (10 mg) given to the mother. The fetus was removed, blotted dry, and weighed. The fetus was then killed with pentobarbital sodium (2 ml, ~250 mg/kg). Fetal, placental, and sectioned heart weights were recorded. The common right and left carotid arteries were dissected from the base of the carotid branch to the base of the skull (CON, $n = 10$; PI-IUGR, $n = 8$). The umbilical arteries were dissected from the umbilical cord between the fetal insertion site and the placental branches (CON, $n = 12$; PI-IUGR, $n = 9$). Arteries were stored in calcium-free phosphate-buffered saline at 4 °C until testing. Preliminary samples of control and PI-IUGR carotid and umbilical arteries were processed for histology. These preliminary histological samples were fixed using 10% neutral-buffered formalin, dehydrated by ethanol, and embedded in paraffin. The arteries were sectioned at 5 μm with each artery stained with Movat's pentachrome for ground substance or sulfated GAGs, fibrin, muscle, collagen, and elastin content.

A 2-mm-long ring portion of the dissected arteries was measured for thickness and inner diameter optically. The dissected artery was then cannulated and sutured. Arteries were then tested for passive compliance in a custom arteriography chamber that allowed the large vessels to be stretched to *in vivo* length, pressurized, and imaged. Calibrated pressure transducers (Living Systems Instruments, LSI; Burlington, VT) were placed on the upstream and downstream sides of the vessel and were recorded using the WinDaq data acquisition software (Dataq Instruments; Akron, OH). The vessels were statically pressurized with calcium-free phosphate-buffered saline solution using a Cole-Parmer Masterflex pump (Vernon Hills, IL) from 5 to 10–200 mm Hg in 10 mm Hg increments, held to allow stress relaxation, and imaged using a Canon Rebel XSi digital camera of 14.5 μm resolution (Lake Success, NY). Transmural pressure and the outer diameter were recorded using a custom-written Matlab (MathWorks, Natick, MA) image processing script. Following mechanical testing, arterial segments were frozen for biochemical assay and segments fixed for histological examination as described below.

In Vitro Biochemical Assays

An ~20 mg portion per arterial sample was lyophilized and weighed for dry mass. The dried tissue was hydrolyzed in 200 μl of 6 mol/l HCl and dried using a speedvac. The amounts of elastin and collagen incorporated into the arterial walls of the PI-IUGR sheep were quantified using standard measurements of tissue desmosine and hydroxyproline content, respectively (36,37). An additional ~20 mg portion per arterial sample was dried and weighed for dry mass. Sulfated GAG content was measured using a standard dimethylmethylene assay with chondroitin-6-sulfate (Sigma-Aldrich, St Louis, MO) as the standard (38).

Histology

Mechanical test samples of control and PI-IUGR carotid and umbilical arteries were processed for histology. The histological samples were fixed using 10% neutral-buffered formalin, dehydrated by ethanol, and embedded in paraffin. The arteries were sectioned at 5 μm, with each artery stained with Verhoeff-van Gieson for collagen and elastin content and hematoxylin and eosin for general structure and cell number.

In addition, representative samples were chosen for carotid (CON = 3 and IUGR = 3) and umbilical (CON = 3 and IUGR = 3) arteries for high-resolution SHG imaging. SHG samples were fixed using 10% neutral-buffered formalin, dehydrated by ethanol, and embedded in paraffin. Arteries were sectioned in the axial and circumferential planes at 10 μm. The SHG imaging system consisted of a Zeiss LSM 510 instrument (Carl Zeiss, Oberkochen, Germany) equipped with a tunable pulsed two-photon infrared laser (Chameleon from Coherent, Santa Clara, CA) and external nondescanned photo multiplier tube detectors. Arterial samples were excited with 800 nm via a water immersion objective 40×, 1.4NA Plan-Apochromat (Carl Zeiss). The response signal was split by a dichroic mirror 425 DCLP (Chroma Technologies, Rockingham, VT). The SHG collagen fluorescence was measured using a narrow band pass filter HQ400/20m-2p (Chroma Technologies) and elastin fluorescence with a broad visible band pass filter HQ575/250m-2p (Chroma Technologies). The images were examined in a blinded fashion for qualitative differences between the control and PI-IUGR groups.

Data Analysis

Biomechanical data are presented as mean ± SEM for the transmural pressure and the diameter stretch ($\lambda = d/d_o$, where d is the current diameter and d_o is the initial diameter). The transition stretch (λ_{trans}) describes both the elastin content and/or organization of the artery and the engagement point of collagen. For the mechanical measures, experimental pressure (p) and diameter stretches (λ) were fit using an exponential nonlinear least squares method to give an r^2 value ≥0.90. The λ_{trans} from the nearly linear elastin region to the collagen engagement region was found by a 5% change in the slope, as has been previously reported (39).

The Verhoeff-van Gieson images were used to quantify the elastin area fraction in Matlab (MathWorks) by an intensity threshold to find the artery wall area followed by a threshold of the artery wall to find the darker elastin band areas. The hematoxylin and eosin images quantified cellular content (nuclei number per vascular area) using a custom-written Matlab script to identify the number of cell nuclei using a threshold in the blue–yellow axis in the L*a*b* color space per artery wall area using an intensity threshold.

Statistical significance of the biomechanical characteristics was found using a mixed-model ANOVA with terms for sex, treatment (CON vs. PI-IUGR), and a random animal term to account for repeated pressure and diameter measurements made in the same fetal vessel. Other measurements were examined using a two-sided Student's t-test assuming unequal variance for parametric data and a Mann–Whitney test for nonparametric data as noted. A value of $P < 0.05$ was considered to be significant.

ACKNOWLEDGMENTS

The authors thank Laura Brown and Stephanie Thorn for providing tissue, expertise, and assistance in using the PI-IUGR model. In addition, we thank the staff at the Perinatal Research Center at the University of Colorado School of Medicine for their assistance and resources for this project. Biochemical assays were run under the advisement of Ivan Stoilov and Robert Mecham, Department of Cell Biology and Physiology, Washington University School of Medicine, St. Louis, MO. The authors thank Kurt Stenmark at the Anschutz Medical Campus for many helpful conversations about this article. SHG images were taken with the expertise at the Advanced Light Microscopy Core, School of Medicine, University of Colorado, Denver.

STATEMENT OF FINANCIAL SUPPORT

This project was funded in part by the American Heart Association Pacific Mountain Predoctoral Fellowship; Sigma Xi Grants in Aid; National Institutes of Health grants 1K08HD060688-1, 1R01DK088139-01A1, and 1K25 HL094749; Center for Women's Health Research; and the University of Colorado Junior Faculty Research Development Award.

REFERENCES

1. Kobs RW, Chesler NC. The mechanobiology of pulmonary vascular remodeling in the congenital absence of eNOS. Biomech Model Mechanobiol 2006;5:217–25.
2. Safar ME, Levy BI, Struijker-Boudier H. Current perspectives on arterial stiffness and pulse pressure in hypertension and cardiovascular diseases. Circulation 2003;107:2864–9.
3. Shadwick RE. Mechanical design in arteries. J Exp Biol 1999;202(Pt 23):3305–13.
4. Faury G. Function-structure relationship of elastic arteries in evolution: from microfibrils to elastin and elastic fibres. Pathol Biol 2001;49:310–25.
5. Burkhardt T, Matter CM, Lohmann C, et al. Decreased umbilical artery compliance and IGF-I plasma levels in infants with intrauterine growth restriction – implications for fetal programming of hypertension. Placenta 2009;30:136–41.
6. Wagenseil JE, Mecham RP. Vascular extracellular matrix and arterial mechanics. Physiol Rev 2009;89:957–89.
7. Wells SM, Langille BL, Lee JM, Adamson SL. Determinants of mechanical properties in the developing ovine thoracic aorta. Am J Physiol 1999;277(4 Pt 2):H1385–91.
8. Barry JS, Rozance PJ, Anthony RV. An animal model of placental insufficiency-induced intrauterine growth restriction. Semin Perinatol 2008;32:225–30.
9. Galan HL, Anthony RV, Rigano S, et al. Fetal hypertension and abnormal Doppler velocimetry in an ovine model of intrauterine growth restriction. Am J Obstet Gynecol 2005;192:272–9.
10. Barker DJ. Intrauterine programming of adult disease. Mol Med Today 1995;1:418–23.
11. Thornburg KL, Louey S. Fetal roots of cardiac disease. Heart 2005;91:867–8.
12. Barry JS, Anthony RV. The pregnant sheep as a model for human pregnancy. Theriogenology 2008;69:55–67.
13. Boer RD. *Trends in Continuum Mechanics of Porous Media*. Springer: Norwell, MA, 2005.
14. Et-Taouil K, Safar M, Plante GE. Mechanisms and consequences of large artery rigidity. Can J Physiol Pharmacol 2003;81:205–11.
15. Mahmud A, Feely J. Arterial stiffness and the renin-angiotensin-aldosterone system. J Renin Angiotensin Aldosterone Syst 2004;5:102–8.
16. Briones AM, Arribas SM, Salaices M. Role of extracellular matrix in vascular remodeling of hypertension. Curr Opin Nephrol Hypertens 2010;19:187–94.
17. Kelleher CM, McLean SE, Mecham RP. Vascular extracellular matrix and aortic development. Curr Top Dev Biol 2004;62:153–88.
18. O'Connell MK, Murthy S, Phan S, et al. The three-dimensional micro- and nanostructure of the aortic medial lamellar unit measured using 3D confocal and electron microscopy imaging. Matrix Biol 2008;27:171–81.
19. Holzapfel G, Gasser T, Ogden R. A new constitutive framework for arterial wall mechanics and a comparative study of material models. J Elasticity 2000;61:1–48.
20. Eberth JF, Popovic N, Gresham VC, Wilson E, Humphrey JD. Time course of carotid artery growth and remodeling in response to altered pulsatility. Am J Physiol Heart Circ Physiol 2010;299:H1875–83.
21. Wagenseil JE, Ciliberto CH, Knutsen RH, Levy MA, Kovacs A, Mecham RP. Reduced vessel elasticity alters cardiovascular structure and function in newborn mice. Circ Res 2009;104:1217–24.
22. Thompson JA, Richardson BS, Gagnon R, Regnault TR. Chronic intrauterine hypoxia interferes with aortic development in the late gestation ovine fetus. J Physiol (Lond) 2011;589(Pt 13):3319–32.
23. Thompson JA, Gros R, Richardson BS, Piorkowska K, Regnault TR. Central stiffening in adulthood linked to aberrant aortic remodeling under suboptimal intrauterine conditions. Am J Physiol Regul Integr Comp Physiol 2011;301:R1731–7.
24. Martyn CN, Greenwald SE. A hypothesis about a mechanism for the programming of blood pressure and vascular disease in early life. Clin Exp Pharmacol Physiol 2001;28:948–51.
25. Nilsson PM, Lurbe E, Laurent S. The early life origins of vascular ageing and cardiovascular risk: the EVA syndrome. J Hypertens 2008;26:1049–57.
26. Norman M. Low birth weight and the developing vascular tree: a systematic review. Acta Paediatr 2008;97:1165–72.
27. Rondó PH, Lemos JO, Pereira JA, Oliveira JM, Innocente LR. Relationship between birthweight and arterial elasticity in childhood. Clin Sci 2008;115:317–26.

28. Laurent S, Boutouyrie P, Asmar R, et al. Aortic stiffness is an independent predictor of all-cause and cardiovascular mortality in hypertensive patients. Hypertension 2001;37:1236–41.
29. Díez J. Arterial stiffness and extracellular matrix. Adv Cardiol 2007;44:76–95.
30. Domanski MJ, Mitchell GF, Norman J, Exner D, Pitt B, Pfeffer MA. Independent prognostic information provided by sphygmomanometrically determined pulse pressure and mean arterial pressure in patients with left ventricular dysfunction. Circulation 1998 98:225.
31. Stefanadis C, Dernellis J, Tsiamis E, et al. Aortic stiffness as a risk factor for recurrent acute coronary events in patients with ischaemic heart disease. Eur Heart J 2000;21:390–6.
32. Eriksson JG, Forsén T, Tuomilehto J, Winter PD, Osmond C, Barker DJ. Catch-up growth in childhood and death from coronary heart disease: longitudinal study. BMJ 1999;318:427–31.
33. Meyer K, Lubo Zhang. Fetal programming of cardiac function and disease. Reprod Sci 2007;14:209–16.
34. Rozance PJ, Crispo MM, Barry JS, et al. Prolonged maternal amino acid infusion in late-gestation pregnant sheep increases fetal amino acid oxidation. Am J Physiol Endocrinol Metab 2009;297:E638–46.
35. Rozance PJ, Limesand SW, Barry JS, Brown LD, Hay WW Jr. Glucose replacement to euglycemia causes hypoxia, acidosis, and decreased insulin secretion in fetal sheep with intrauterine growth restriction. Pediatr Res 2009;65:72–8.
36. Sims TJ, Bailey AJ. Quantitative analysis of collagen and elastin cross-links using a single-column system. J Chromatogr 1992;582:49–55.
37. Starcher B, Conrad M. A role for neutrophil elastase in the progression of solar elastosis. Connect Tissue Res 1995;31:133–40.
38. Farndale RW, Sayers CA, Barrett AJ. A direct spectrophotometric microassay for sulfated glycosaminoglycans in cartilage cultures. Connect Tissue Res 1982;9:247–8.
39. Lammers SR, Kao PH, Qi HJ, et al. Changes in the structure–function relationship of elastin and its impact on the proximal pulmonary arterial mechanics of hypertensive calves. Am J Physiol Heart Circ Physiol 2008;295:H1451–9.